13th World Conference on Earthquake Engineering
Vancouver, B.C., Canada
August 1-6, 2004
Paper No. 1930

DENSIFICATION OF SATURATED SILTY SOILS USING COMPOSITE STONE COLUMNS FOR LIQUEFACTION MITIGATION

T. SHENTHAN[1], S. THEVANAYAGAM[2] and G. R. MARTIN[3]

SUMMARY

Vibro stone column is a proven technique to mitigate liquefaction and its consequences in saturated sandy soils. This technique relies mainly on three mechanisms: (a) densification of insitu soil during installation, (b) reinforcement, and (c) drainage during an earthquake to hinder excess pore pressure development. However, its effectiveness is limited in low-permeable silty soils that are prone to liquefaction. Composite stone column technique is a recent modified vibro-stone column technique with supplementary wick drains to enhance densification of such silty soils, and thereby, mitigate liquefaction-induced hazards. In this technique, wick drains are pre-installed at midpoints between designated stone column locations. Wick drains aid dissipation of excess pore pressure induced during installation enhancing further densification. This paper presents a numerical model to simulate, and to analyze soil densification during composite stone column installation. Numerical results for densification performance of composite stone column during installation are presented and compared with field performance data. Key soil parameters that limit the effectiveness of composite stone columns for densification during installation are identified.

INTRODUCTION

Liquefaction has been a matter of great interest in geotechnical engineering for more than three decades. It is one of the primary causes of lateral spreading, failures of bridge foundations, embankments, and ports and harbor facilities during earthquakes (e.g. 1964 Alaska earthquake, 1995 Kobe earthquake). Vibro-stone column method (Fig.1a) is proven ground improvement technique for liquefaction mitigation and foundation strengthening in sands containing less than 15% passing sieve #200 (74 μm) and less than 2% of clayey particles (<2 μm) (FHWA [1]). Saturated loose to medium dense sands densify due to vibration and/or impact-induced liquefaction and the associated expulsion of pore water from the soil through the surrounding stone columns during vibro-stone column installation. The densified soil is more resistant to liquefaction, and has performed well during earthquakes (Mitchell [2], Andrus and Chung [3]). Stone columns also serve as reinforcing elements and help reduce the seismic shear stress intensity experienced by soils surrounding the stone columns (Baez [4], Baez [5]). During earthquakes, the stone columns serve as pathways for drainage of pore water and help relieve seismic induced excess pore pressures as well.

[1] Ph.D. Candidate, State University of New York at Buffalo, USA. Email: shenthan@eng.buffalo.edu
[2] Assoc. Prof., State University of New York at Buffalo, USA. Email: theva@eng.buffalo.edu
[3] Prof., University of Southern California, USA. Email: geomar@usc.edu

Based on field data, Baez [4] outlines an empirical approach (Fig.7, introduced later) for design of vibro-stone columns (Fig.1a) to improve sandy soils, containing less than 15% silt. No detailed analytical procedures are available to determine the densification achievable during stone column installation or the effects of various construction choices such as stone column spacing and diameter on the degree of improvement. The current state of practice depends mainly on previous experience or field test programs to determine the applicability of the technique and choice of stone column spacing, etc. at a given site. If the soil contains excessive fines, it has been considered difficult to densify using vibro-stone columns. However, recent case histories show that pre-installed supplementary wick drains (Fig.1b) relieve excess pore pressures developed during stone column installation and dynamic compaction in silty soils (Andrews [6], Dise [7], and Luehring [8]) and enhance densification during installation. Again, no analytical procedures or design guidelines are available to date to address such a composite vibro-stone column.

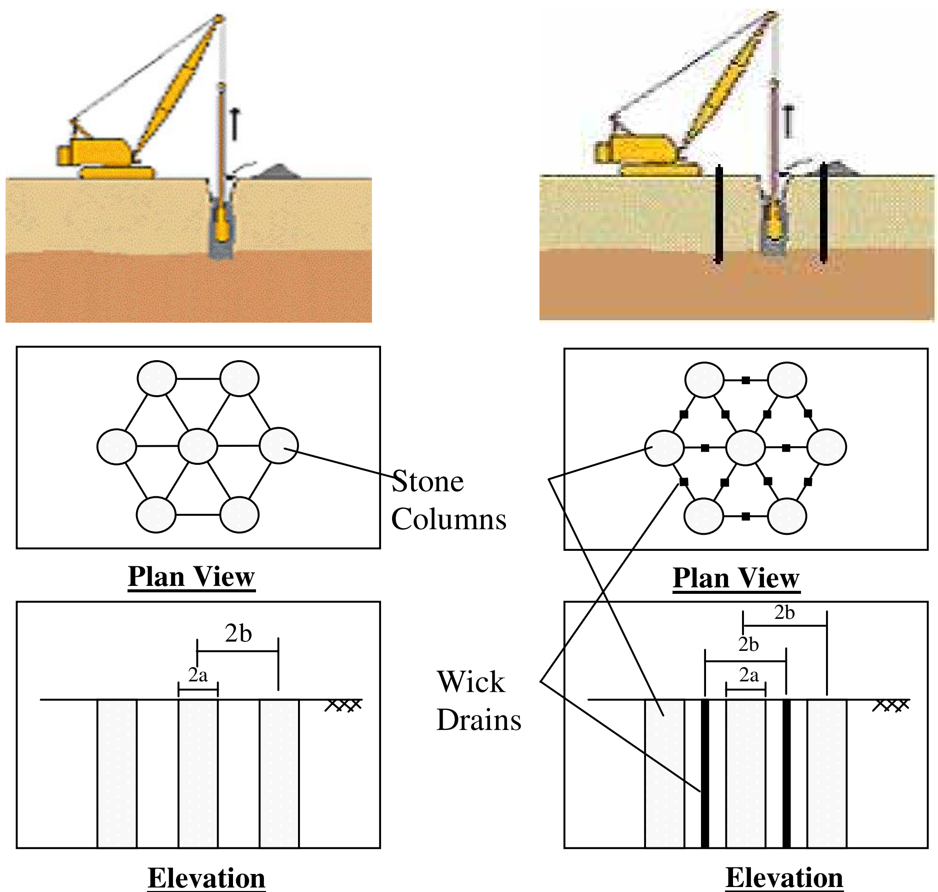

(a) Traditional Vibro-stone Column (b) Composite Vibro-stone column

Fig.1 Vibro-Stone Columns and Composite Vibro-Stone Column

Vibro-Stone Column Installation Process

Vibro-stone column installation process involves insertion of a vibratory probe with rotating eccentric mass (FHWA [1]) (Fig.2a). The probe plunges into the ground due to its self-weight and vibratory energy, which facilitates penetration of the probe. Once the specified depth (depth of stone column) is reached, the probe is withdrawn in steps (lifts) of about 1m. During withdrawal of the probe, the hole is backfilled with gravel. During each lift the probe is then reinserted expanding the stone column diameter. This process is repeated several times until a limiting condition is achieved. In sandy soils, the limiting condition is considered to be achieved when the electric current amperage supply reading to the vibratory probe reaches a high value during reinsertion of the probe, indicating high resistance to penetration into the stone column. This reading is an indirect indication of the extent of the stone column, and soil density around the stone column. In cases where the amperage readings do not reach high limiting amperage values, construction proceeds until a minimum amount of stones is introduced into the ground to reach a specified minimum stone-column diameter. This happens almost invariably in very low permeable soils. It is suspected that this occurs due to lack of sufficient drainage and low densification of the soil around the stone column during installation works.

In saturated soils, soil densification occurs due to two phenomena during stone column installation: (a) during insertion of the vibratory probe, excess pore water pressure is induced in the soil surrounding the probe, and concurrent dissipation occurs leading to soil densification; and (b) expansion of a zero cavity and subsequent cavity expansions during repeated fillings of the cavity by stones and probe insertions cause significant excess pore water pressures, and concurrent consolidation and soil densification. The extent of the densified soil zone surrounding the probe depends on many factors including the stone column diameter, energy imparted by the probe, vibratory duration, and drainage boundary conditions. Faster the dissipation allowed, higher the density that could be achieved for the same duration of vibration for the same stone column diameter.

THEORETICAL BACKGROUND

Energy Dissipation and Pore Pressure Generation

During installation process of stone columns the probe is continuously vibrated imparting energy into the surrounding soil. In this paper the energy source in the probe is considered as an in-depth point-source (Fig.2b), and the energy propagates spherically outward. It is further assumed that there is no energy loss within a spherical region of radius r_0, where r_0 is the radius of the probe. Let the energy imparted by the probe into the soil per unit time be W_0. Energy delivered at the probe-soil interface attenuates due to: (i) geometrical damping, and (ii) material damping. Generally, attenuation relationship for vibration amplitude due to material damping for ground vibration is of the form $A=A_1\exp[-\alpha(r-r_1)]$, where, A_1 is amplitude at distance r_1 from the source, A is amplitude at distance r from the source, and α is the coefficient of attenuation. α depends on several factors such as source characteristics, frequency of vibration, wave velocity, soil profile, stress and strain field within the surrounding soil, soil type, degree of saturation, changes in excess pore pressure and soil density during vibration, etc. Ground vibration studies indicate that, typically, α ranges from 0.02~0.26 m^{-1} (Richart [9], Dowding [10]). Assuming that the attenuation relationship due to material damping presented before applies to vibroflotation and considering radial damping, the energy density at a radius r is given by:

$$W = \frac{W_0}{4\pi r^2}\exp\left[-2\alpha\left(r-r_0\right)\right] \tag{1}$$

where, W = energy per unit time passing through a unit area of the spherical surface at radius r. α was assumed to be 0.13 m^{-1}, for the simulations reported herein. Energy loss per unit time per unit volume of soil at distance r is,

$$w = W_0\frac{\alpha}{2\pi r^2}Exp\left[-2\alpha\left(r-r_0\right)\right] \tag{2}$$

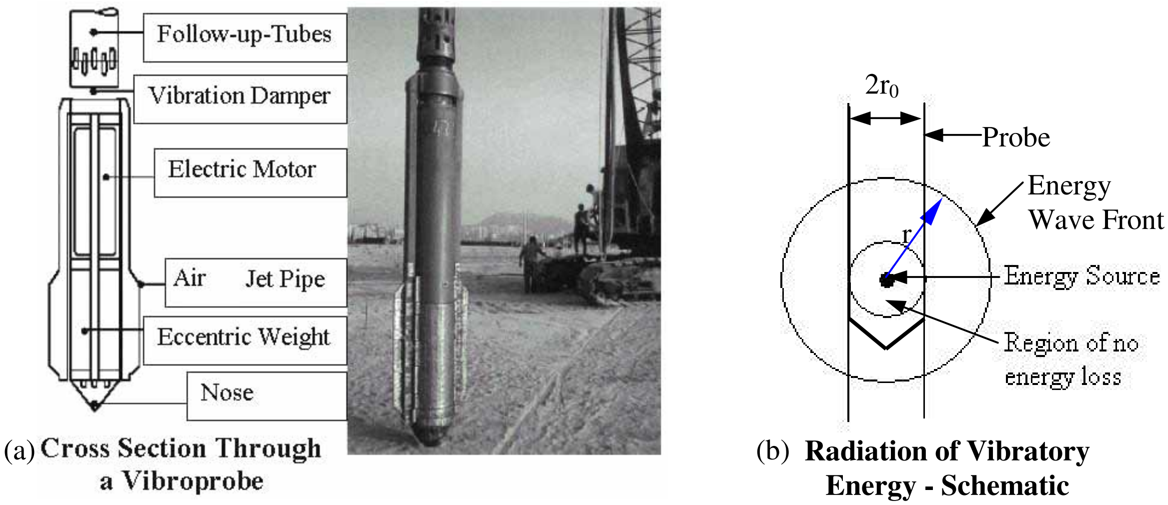

Fig.2 The Vibratory Probe and Energy Propagation

In the soil around the vibratory probe, as excess pore pressure develops due to vibration, the soil becomes weak. Since the amplitude of vibration of the probe is limited (FHWA [1]), the energy imparted to the surrounding soil would decrease resulting in a reduced efficiency. When the pore pressures dissipate, and the soil is sufficiently densified, the energy transfer rate would increase. In this paper, this phenomenon was taken into account considering the energy transfer rate to decay with increasing excess pore pressure:

$$w = W_0 \frac{\alpha}{2\pi r^2} Exp\left[-2\alpha\left(r - r_0\right)\right].Exp\left[-\beta\left(r_u\right)_{av}\right] \tag{3}$$

where, $W_o = \eta_0 P_0$, P_0= power rating of the vibratory probe, η_0=probe efficiency, $(r_u)_{av}$=the average excess pore pressure ratio within the soil surrounding the probe up to an effective radial distance r_e, and β=a constant.

Based on a large experimental database and theoretical considerations, excess pore water pressure generated due to cyclic loading has been related to frictional energy loss in the soil by Thevanayagam [11] as:

$$r_u = 0.5 Log_{10}\left(100 \frac{E_c}{E_L}\right), \qquad \frac{E_c}{E_L} > 0.05 \tag{4}$$

where, r_u=excess pore pressure ratio (u/σ_0'), σ_0'=initial mean effective confining pressure, E_c = cumulative energy loss per unit volume of soil, and E_L = energy per unit volume required to cause liquefaction.

Cavity Expansion and Pore Pressure Generation

Initial insertion of the probe into the ground can be considered as expanding a zero cavity to a diameter the same as that of the probe. Filling of this cavity by stones and inserting the probe further expands the cavity by pushing the stone backfill radially outwards. Lifting the probe causes slight contraction of the cavity. These are schematically shown in Figs.3a, b, and c, respectively. Repeated lifting, filling, and insertion of the probe cause repeated cavity expansions. Consider the soil to be an elastic-perfectly plastic material with an undrained shear strength of S_u under an initial horizontal stress of σ_{h0}. A, C, and E in Fig.3 are material points in a horizontal plane. When the probe is inserted, a cavity of radius R_e is created, and the soil is pushed away radially. Soil between A and E has deformed plastically, while the soil beyond E has undergone only small, elastic deformations. When the probe is withdrawn (or passes below the point A), soil unloads elastically until a condition for reverse plasticity is reached at point A, and further unloads until the plastic region just reaches point C. Figs.3d, and e illustrate the changes in radial and shear stresses within the soil during loading and unloading.

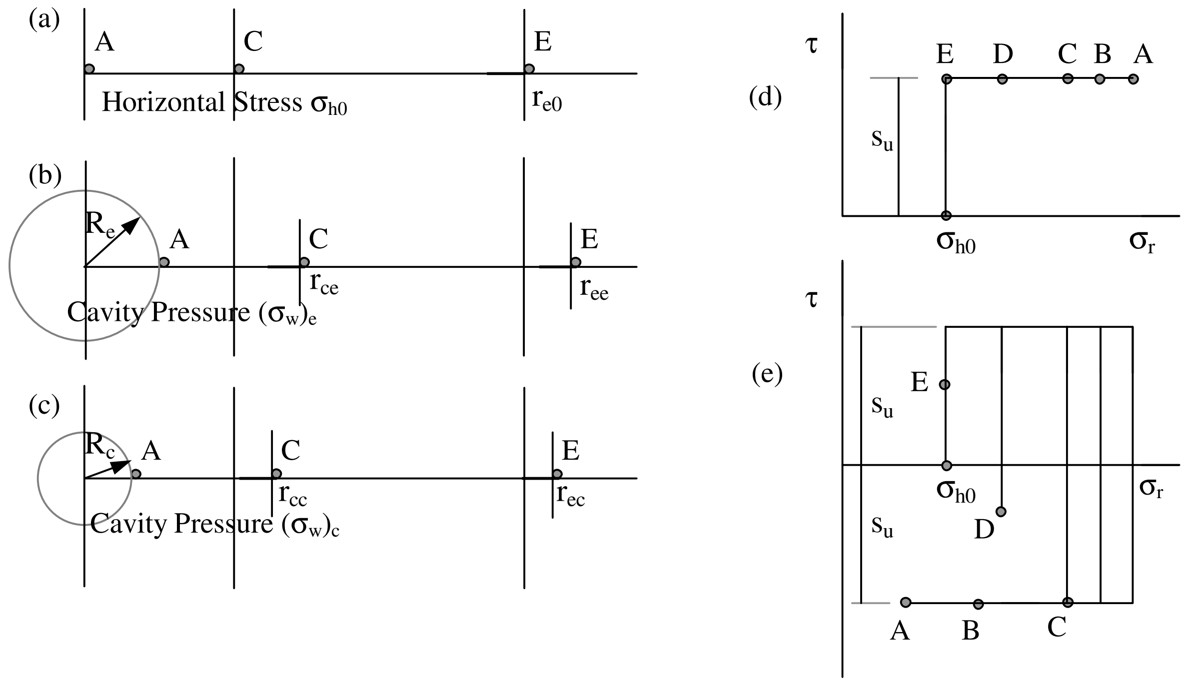

Fig.3 Definition of Radii Used in Analysis, and Stress States Around the Vibratory Probe
(a) Initial condition; (b) After vibratory probe installation; (c) After the probe passed/removed from the depth of concern, i.e. during cavity contraction; (d) Stress states around the probe corresponding to stage-b; and, (e) Stress states corresponding to stage-c

Excess pore pressure generated during initial cavity expansion (Fig.3b) is given by:

$$u_e = 2S_u \ln\left[\frac{r_{ee}}{r}\right] \quad for \quad r \le r_{ee}$$
$$0 \quad for \quad r > r_{ee} \tag{5}$$

where, u_e is excess pore pressure, r is radial distance, and r_{ee} is radial distance of the elastic-plastic boundary (point E in Fig.3b) during expansion (Appendix A). After cavity contraction, excess pore pressure, for any value of r, will be:

$$u_e = 0.5\left(\sigma_r(r) + \sigma_\theta(r) - 2\sigma_{h0}\right) \tag{6}$$

where, σ_r and σ_θ are radial and angular stresses. Since there is no excess pore pressure generated beyond the material point E, which remains in the elastic region during contraction, the value of excess pore pressure from Eq.6 will be zero for $r>r_{ec}$ (Appendix A). Details of the derivation of the above equations is presented in Shenthan [12].

In order to account for elasto-plastic behavior of soils, one must also add the shear-induced pore pressure component to the above elastic-perfectly plastic solutions given by Eqs.5, and 6. Thevanayagam [13] studied undrained behavior of loose sand and sandy silt mixes and proposed a simple relationship between shear induced pore pressures, relative density, and initial effective confining pressure (σ_0'). The shear induced pore pressure normalized by the initial mean effective confining stress was termed as collapse potential (CP). Fig.4 shows this relationship. The notation '100-OS15' means test results for the specimen prepared by mixing Ottawa sand (F55, US Silica Co., IL) with 15% by dry weight of silt (sil co sil#40, US Silica Co., IL), and tested under 100 kPa initial effective confining pressure. The shear induced pore pressure component is given by,

$$u_{sh} = CP * \sigma_0^{'} \tag{7}$$

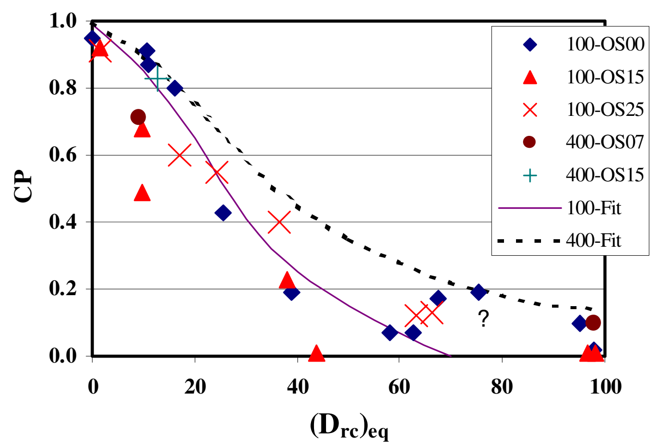

Fig.4 CP vs. Equivalent Relative Density

Shear induced pore pressure is included only for the plastically deformed region. Combining Eqs.5 and 7, total excess pore pressure during cavity expansion is given by:

$$u_e = \begin{cases} 2S_u \ln\left[\dfrac{r_{ee}}{r}\right] + u_{sh} & for \quad r \le r_{ee} \\ 0 & for \quad r > r_{ee} \end{cases} \tag{8}$$

And for cavity contraction,

$$u_e = \begin{cases} 0.5\left(\sigma_r(r) + \sigma_\theta(r) - 2\sigma_{h0}\right) + u_{sh} & for \quad r \le r_{cc} \\ 0.5\left(\sigma_r(r) + \sigma_\theta(r) - 2\sigma_{h0}\right) & for \quad r > r_{cc} \end{cases} \tag{9}$$

where, r_{cc} is radial distance of the elastic-plastic boundary (point C in Fig.3c) during contraction (Appendix A).

Pore Pressure Dissipation and Densification

Neglecting dissipation in the vertical direction, in order to reduce the computational time, the governing equation for pore pressure dissipation in the soil surrounding the vibro-stone column system is:

$$\frac{\partial u}{\partial t} = \frac{k_h}{\gamma_w m_v}\left(\frac{\partial^2 u}{\partial r^2} + \frac{1}{r}\frac{\partial u}{\partial r} + \frac{1}{r^2}\frac{\partial^2 u}{\partial \theta^2}\right) + \frac{\partial u_g}{\partial t} \tag{10}$$

where k_h is the hydraulic conductivity of the soil in the horizontal direction; m_v=volume compressibility of the soil; u=excess pore water pressure at coordinates (r, θ); t=time; γ_w=unit weight of water; r, and θ are radial, and angular coordinates, respectively. The term u_g stands for time dependent pore pressure generation as in the case due to vibratory energy. In the case of cavity expansion, excess pore pressure is assumed to change instantaneously corresponding to expansion of contraction. Volumetric densification of a soil element due to excess pore pressure dissipation may be obtained by:

$$\varepsilon_v = \int m_v . d\sigma' \tag{11}$$

where ε_v=volumetric strain, and σ'=mean effective confining pressure. Seed [14] suggest that m_v values for sands increase from its initial value according to the following relationship, and do not decrease from the highest value obtained:

$$\frac{m_v}{m_{v0}} = \frac{\exp(y)}{1 + y + y^2/2} \geq 1; \quad y = a.r_u^b; \quad a = 5(1.5 - D_r); \quad b = 3(4)^{-D_r} \tag{12}$$

where, m_v and D_r are initial volume compressibility and relative density of soils, respectively. The above equation is modified to use equivalent relative density $(D_r)_{eq}$ based on intergrain contact considerations (Shenthan [12, 15]) instead of D_r to account for the effects of silt content.

Two sets of numerical simulations were conducted to study densification process of soils during stone column installation. In the first set of simulations, the effect of cavity expansion was neglected and the effect of vibration induced pore pressure generation and dissipation was considered. In this case, u_g in Eq.10 was updated based on Eqs. 3 and 4. Further, based on experimental data available, hydraulic conductivity k was also obtained as a function of silt content. In the second set of simulations, the effect of cavity expansion was included and the vibration induced pore pressures were neglected. In this case, u_g in Eq.10 was updated using Eqs.8 and 9. These simulations are presented below.

NUMERICAL SIMULATIONS

Energy Dissipation and Densification

The simulations presented herein consider soil densification due to dissipation of vibration induced pore pressures only. Fig.5 shows a composite vibro-stone column layout. The radii of the stone columns and wick drains are a and r_w, respectively. The spacing between stone columns is 2b. The spacing between wick drains is b. The wick drains are installed first, and the surrounding stone-columns are installed next followed by installation of the center column. The numerical simulation presented in the following sections pertains to densification of the soil during installation of the center column. Using Eqs. 4, and 10 through 12, a finite-difference numerical scheme was developed to simulate this densification process in the soil surrounding the center column. Boundaries of symmetry allow reducing the computational time by requiring calculations to be done for only the representative area shown in Fig.5.

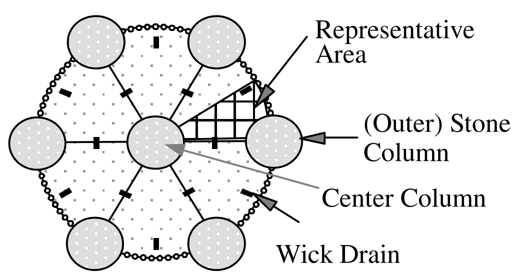

Fig.5 Composite Stone Column Layout

Vibro-stone Columns without Wicks

The simulations herein consider installation of vibro-stone columns in clean sand with no wick drains (Fig. 1a). Three different initial densities were used: (a) D_r=40%, (b) D_r=48%, and (c) D_r=59%. Three different area replacement ratios (A_r=5.6, 10.0, and 22.5%) were assumed for each initial density, where $A_r=(A_c/A_e)*100\%$, A_c is area of the stone-column, A_e is the tributary area ($=\pi*D_e^2/4$), and D_e=equivalent diameter of the tributary area=1.053 times the center-to-center spacing between stone columns installed in a triangular pattern. These A_r values correspond to center-to-center stone column spacing of 4 diameters, 3 diameters, and 2 diameters, respectively. The hydraulic conductivity was assumed to be $5x10^{-6}$ m/s. Table 1 summarizes the probe characteristics used for the simulation. Table 2 summarizes simulation parameters. The post-improvement densification results are shown in Fig.6a.

Table 1 Vibratory Probe Specifications

Length m	Frequency Hz	Power Rating P_0 kW	η_0 %	β	Avg. Penetration Rate cm/s
3	50	120	50	4	3

Table 2 Simulation Parameters

Column Dia. (m)	Column Spacing (m)			k (m/s)
	A_r=5.6%	10.0%	22.5%	
0.9	3.6	2.7	1.8	$5*10^{-6}$

Note: Initial effective confining pressure at the depth considered is about 100 kPa.

The area replacement ratio has a significant influence on post-improvement density. This influence diminishes as the initial density increases. Although not shown in this paper, it was also found that hydraulic conductivity plays an important role and higher hydraulic conductivity leads to higher densification for the same vibratory duration (Shenthan [12], Thevanayagam [16]).

For qualitative comparison purposes, the data in Fig.6a may be converted to equivalent SPT blow counts $(N_1)_{60,c-s}$ using Tokimatsu [17] relationship for clean sands, as shown in Fig.6b. This can be compared with the field-case history database for pre- and post-improvement SPT blow counts compiled by Baez [4] shown in Fig.7. The regression curves for post-improvement SPT blow counts obtained by Baez [4] were based on an analysis of a number of case histories, where vibro-stone columns were used to improve sandy soil sites with less than 15% silts. Although direct comparisons are not possible, due to lack of site-specific data, the trend found in Fig.6b agrees well with the trend in Fig.7. Further work is underway to verify simulation results with field trials.

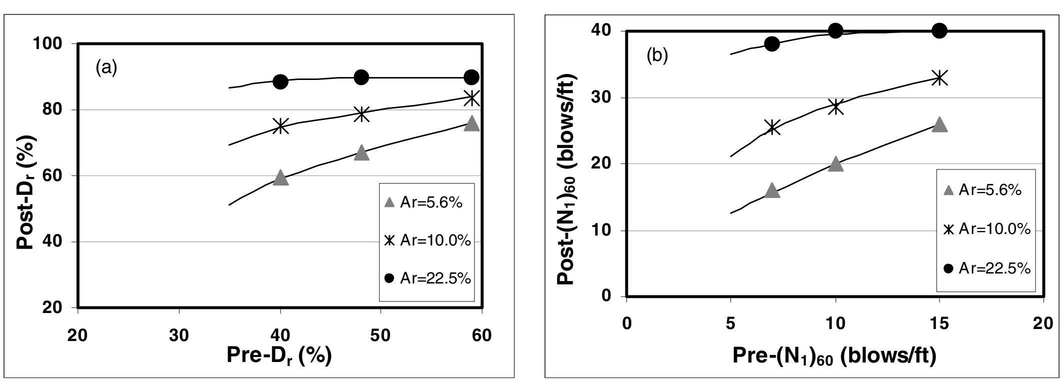

Fig.6 Vibro-Stone Column Simulation Results

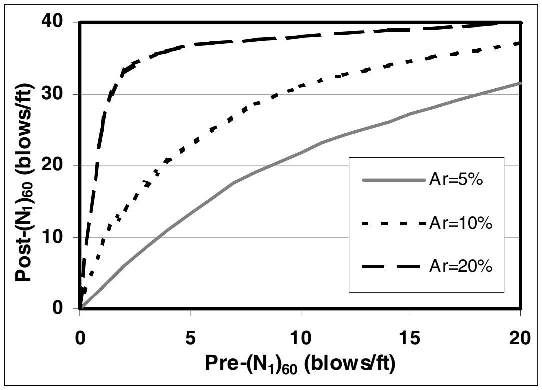

Fig.7 Regression Design Curves (Baez 1995)

Composite Vibro-Stone Column

A number of simulations were conducted to assess the effects of silt content, and area replacement ratio A_r on post improvement density of silty soils supplemented by wick drains (Fig.1b). Three different initial equivalent relative densities ($(D_r)_{eq}$=40, 48 and 59%, Shenthan [12]) were considered. Silt content dependent soil input parameters m_v, k, E_L were obtained from an experimental database for silty soils (Shenthan [15], and Thevanayagam [16]). For direct comparison purposes, the same simulations were repeated for stone columns in the same soil without wick drains (Fig.1a). Figs.8a-c show the simulation results for post-improvement relative densities for A_r=5.6, 10, and 22.5%, respectively, for the three different initial relative densities $(D_r)_{eq}$ considered. Without wick drains, no significant improvement is achieved for soils with hydraulic conductivity less than about 10^{-6} m/s. At low A_r, wick drains do not contribute to any further increase in post-improvement density for all initial densities (Fig.8a). The spacing of stone columns and wick drains is too large and wick drains are far from the stone columns to be effective in reliving the pore pressures during installation and to facilitate repeated cycles of densification. As the area replacement ratio increases, influence of wick drains increases. At high area replacement ratio of about 20% or above (Fig.8c), wick drains significantly contribute to the drainage and repeated densification of silty soils with hydraulic conductivity as low as 10^{-8}m/s. However, the degree of improvement is dependent on hydraulic conductivity.

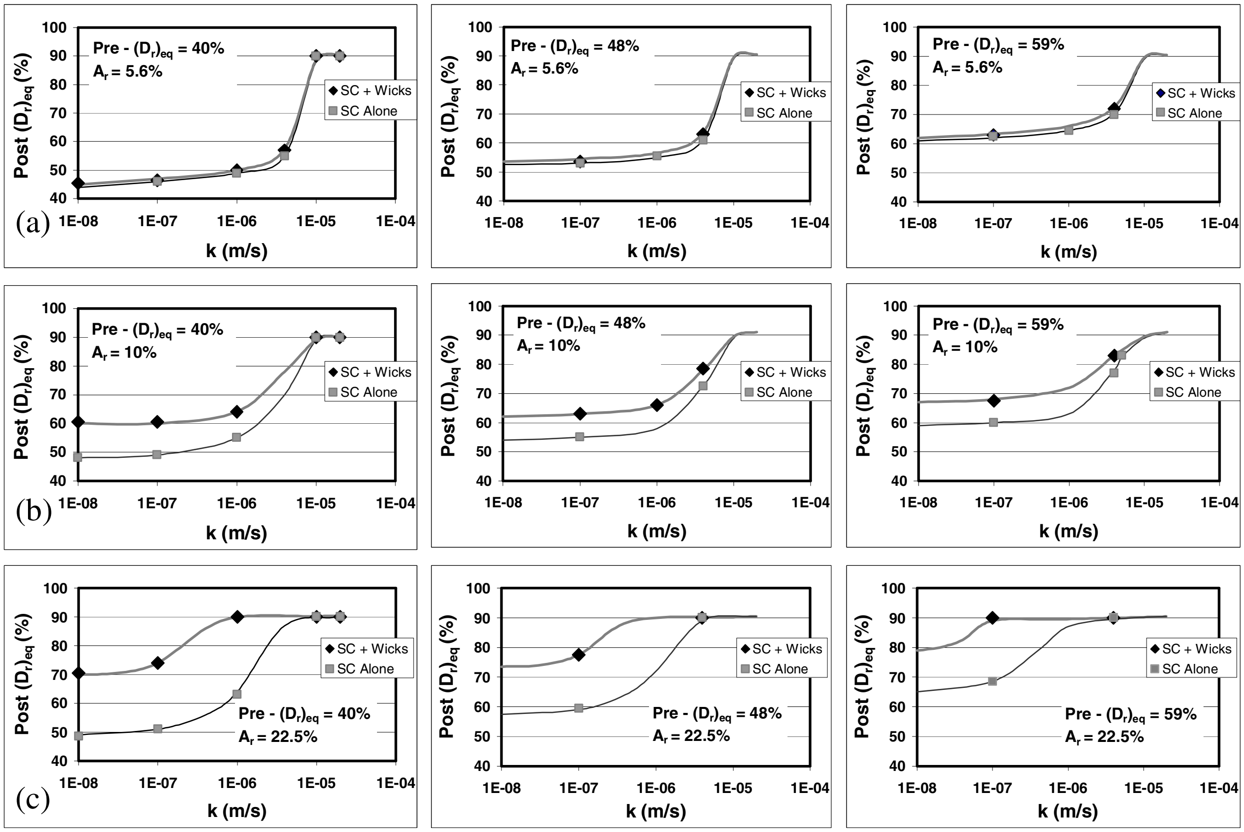

Fig.8 Composite Vibro-Stone Columns – Simulation Results

(SC=Vibro-Stone Column without Wicks, SC + Wicks=Composite Vibro-Stone Column)

Cavity Expansion and Densification

The simulations presented herein consider soil densification due to dissipation of cavity expansion induced pore pressures only. These simulations involved two cases, (a) stone columns with wick drains, and (b) without wick drains. The initial density of soils was $(D_r)_{eq}$=40%. Three different area replacement ratios (A_r=10, 15, and 25%) were considered. Probe characteristics used for the simulation are the same as those summarized in the Table 1. Table 3 summarizes simulation parameters relevant to this analysis. Vibratory probe diameter is 0.36 m. In lifts of 1m, the probe is reinserted 7 times to build a stone column of 0.95m diameter at any given depth. Field observations indicate that this process takes about 4 to 5 minutes per lift of 1m.

Table 3 Simulation Parameters Used in Cavity Expansion

Column Diameter (m)	Column Depth (m)	Column Spacing (m)			Depth Simulated (m)
		A_r=10%	15%	25%	
0.95	15	2.85	2.3	1.8	12

Note: Initial effective confining pressure at the depth considered is about 100 kPa.

The post-improvement densification results are shown in Figs.9a, b, and c for A_r=10, 15, and 25, respectively. Without wick drains, highest improvement is achieved for highly permeable soils at or above 10^{-5}m/s. The post-improvement density depends on hydraulic conductivity and area replacement ratio. Addition of wick drains does not significantly affect the degree of improvement. It appears that the cavity expansion induced pore pressures do not extend far enough from the stone column and hence wick drains do not significantly contribute to drainage in this case, except for large A_r (Fig.9c).

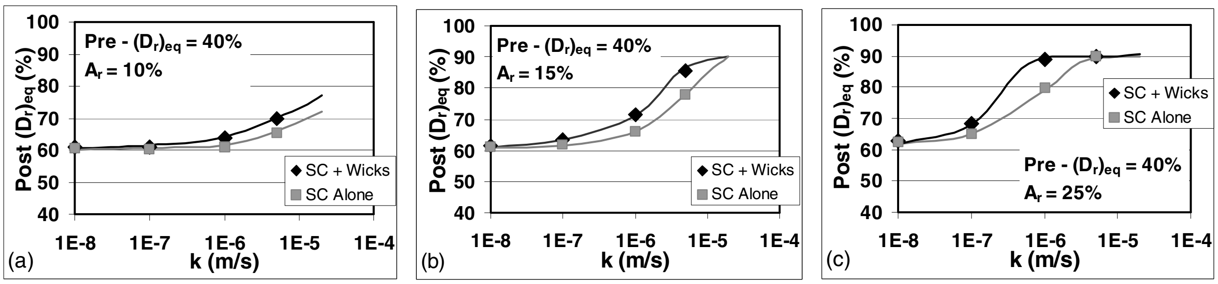

Fig.9 Post-Improvement Densification - Due to pore pressures induced by Cavity Expansion

The above results shown in Figs.8 and 9 indicate that both cavity expansion process and ground vibration contribute to densification. Post-improvement densities due to the coupled effect of both cavity expansion and vibratory energy should be higher than those obtained by considering cavity expansion only. Further work is underway to couple these two phenomena.

CONCLUSION

A numerical model to analyze densification of saturated silty soils during stone column installation has been developed. It includes two phenomena, (a) vibration-induced excess pore pressure development and concurrent dissipation and densification, and (b) cavity expansion-induced excess pore pressure development and concurrent dissipation and densification.

Two factors have been identified important: (i) Area replacement ratio A_r, and (ii) hydraulic conductivity and silt content. Without wick drains, soils at hydraulic conductivities higher than about 10^{-6}m/s may be densified using stone columns alone. Soils with hydraulic conductivities less than 10^{-6}m/s require supplementary wick drains between stone columns. Non-plastic silty soils with hydraulic conductivities as low as 10^{-8}m/s may be improved using close stone column at close spacing of about 2 diameters or less with an area replacement ratio of about 20% or more supplemented with wick drains.

Results reported in this paper pertain to densification due to dissipation of vibration-induced pore pressure, and that due to cavity expansion-induced pore pressure analyzed separately. Post-improvement densities due to the coupled effect of these phenomena should be higher than those obtained by considering cavity expansion only. Additional work is ongoing to couple these two phenomena.

Acknowledgement
Financial support for this research was provided by MCEER Highway Project 094, sponsored by the FHWA.

Appendix A
The radial distance to the elastic-plastic boundary (point E in Fig.3b) r_{ee} during cavity expansion is given by:

$$r_{ee} = R_e \sqrt{I_r} \qquad \text{(A.1)}$$

where, R_e is cavity radius during expansion, and I_r is rigidity index given by G/S_u, where, G and S_u are shear modulus and undrained shear strength, respectively, of the soil. The initial distance of the point E in Fig.3a can be back-calculated by:

$$r_{e0} = \sqrt{r_{ee}^2 - R_e^2} \qquad \text{(A.2)}$$

The radial distance to the elastic-plastic boundary during cavity contraction (point C in Fig.3c) is given by:

$$r_{cc} = R_c \Bigg/ \sqrt{\frac{\exp\left\{\dfrac{2}{I_r}\right\} - 1}{\exp\left\{2\ln\left[\dfrac{R_e}{R_c}\right]\right\} - 1}} \tag{A.3}$$

where, R_c is the cavity radius during contraction.

REFERENCES

1. FHWA. "Stone columns." Ground Improvement Technical Summaries, II. Publication No. FHWA-SA-98-086R. 2001: 71-84.
2. Mitchell JK, Baxter CDP, Munson TC. "Performance of improved ground during earthquakes." Hryciw RD, Editor. Soil improvement for earthquake hazard mitigation, GSP. 49; ASCE, 1995: 1-36.
3. Andrus RD, Chung RM. "Ground improvement techniques for liquefaction remediation near existing lifelines." Building and fire research laboratory, National Institute of Standards and Technology. Report no. 5714. Gaithersburg, 1995.
4. Baez JI. "A design model for the reduction of soil liquefaction by vibro-stone columns" Ph.D. Dissertation. USC, Los Angeles, CA, 1995: 207 p.
5. Baez JI, Martin GR. "Permeability and shear wave velocity of vibro-replacement stone columns." Hryciw RD, Editor. Soil improvement for earthquake hazard mitigation, GSP. 49; ASCE, 1995: 66-81.
6. Andrews DCA. "Liquefaction of silty soils: susceptibility, deformation, and remediation." PhD Dissertation. Department of Civil Engineering, USC, CA, 1998.
7. Dise K, Stevens MG, Von Thun JL. "Dynamic compaction to remediate liquefiable embankment foundation soils." ASCE National Convention, GSP No.45. Reston, VA, 1994: 1-25.
8. Luehring R, Snorteland N, Mejia L, Stevens M. "Liquefaction mitigation of a silty dam foundation using vibro-stone columns and drainage wicks: a case history at salmon lake dam." Proceedings of the 21st USSD annual meeting and lecture. Denver, CO, 2001.
9. Richart FE, Jr, Hall JR, Woods RD. "Vibrations of soils and foundations." Englewood Cliffs, NJ: Prentice-Hall, 1970: 414p.
10. Dowding CH. "Construction vibrations." NJ: Prentice Hall, 1996: 610p.
11. Thevanayagam S, Kanagalingam T, Shenthan T. "Contact density – confining stress – energy to liquefaction." Proceedings of the 15th ASCE Engineering Mechanics Conference. Paper no. 428. Columbia University, NY, 2002.
12. Shenthan T. "Liquefaction mitigation in silty soils using composite stone column." Ph.D. Dissertation. University at Buffalo, Buffalo, NY, 2004: Draft (under review).
13. Thevanayagam S, Shenthan T, Mohan S, Liang J. "Undrained fragility of sands, silty sands and silt." ASCE Journal of Geotechnical & Geoenvironmental Engineering 2002; 128 (10): 849-859.
14. Seed HB, Martin PP, Lysmer J. "The generation and dissipation of pore water pressures during soil liquefaction." Earthquake Engineering Research Center. Report no. UCB/EERC 75-26. UC Berkeley, CA, 1975.
15. Shenthan T. "Factors affecting liquefaction mitigation in silty soils using stone columns." MS Thesis. University at Buffalo, NY, 2001: 220p.
16. Thevanayagam S, Martin GR, Shenthan T, Liang J. "Post-liquefaction pore pressure dissipation and densification in silty soils." Proceedings of the 4th International Conference on Recent Advances in Geotechnical Earthquake Engineering and Soil Dynamics. San Diego, CA, 2001: Paper 4.28.

17. Tokimatsu K, SeedHB. “Simplified procedures for the evaluation of settlements in sands due to earthquake shaking.” Earthquake Engineering Research Center. Report No. UCB/EERC-84/16. UC Berkeley, CA, 1984.